

STRUCTURE AND DYNAMICS OF WATER–SMECTITE INTERFACES: HYDROGEN BONDING AND THE ORIGIN OF THE SHARP O–D_w/O–H_w INFRARED BAND FROM MOLECULAR SIMULATIONS

MAREK SZCZERBA^{1,*}, ARTUR KULIGIEWICZ¹, ARKADIUSZ DERKOWSKI¹, VASSILIS GIONIS²,
GEORGIOS D. CHRYSIKOS², AND ANDREY G. KALINICHEV³

¹ Institute of Geological Sciences, Polish Academy of Sciences, Kraków, Poland

² Theoretical and Physical Chemistry Institute, National Hellenic Research Foundation, Athens, Greece

³ Laboratoire SUBATECH (UMR 6457), Ecole des Mines de Nantes, Nantes, France

Abstract—Experimental studies have shown that a sharp, high-frequency IR band at $\sim 3615\text{ cm}^{-1}$ (in H₂O form) and at $\sim 2685\text{ cm}^{-1}$ (in D₂O form) is a common feature for all smectites, and its position correlates with layer charge. In order to explain the molecular origin of this band in terms of total layer charge, charge localization, as well as nature of interlayer cations influencing the position and intensity of this peak, a series of classical molecular dynamics (MD) simulations was performed for several smectite models. The smectite layers were described using a modified *CLAYFF* force field, where the intramolecular vibrations of H₂O were described more accurately by the Toukan-Rahman potential. The power spectra of molecular vibrations of hydrogens were calculated for selected sub-sets of interlayer H₂O to analyze quantitatively their contribution to the observed spectral features. The statistics of hydrogen bonds in the smectite interlayers were also analyzed to support the spectral calculations.

The simulation results demonstrated clearly that only the H₂O molecules in close proximity to the smectite surface are responsible for the sharp vibrational band observed. Other hypotheses for the possible origins of this band were considered carefully and eventually rejected. Two orientations of H₂O molecules donating one or two H bonds to the basal oxygens of the smectite surface (monodentate and bidentate orientations, respectively) were observed. In both orientations, these H bonds are quite weak, pointing to a generally hydrophobic character of the smectite surface. Both orientations contributed to the high-frequency band, but the monodentate orientation provided the predominant contribution because surface H₂O molecules in this orientation were much more abundant. In good agreement with experiment, only a small difference in the peak position was observed between smectites with different charge localization. The effect of the total layer charge, *i.e.* the red-shift for higher-charge smectites, was also confirmed. This shift arose from the decrease in the H-bonding distances of H₂O in monodentate and bidentate orientation.

Key Words—Adsorbed Water, Clay–Water Interface, Infrared Spectroscopy, Molecular Dynamics, Smectite.

INTRODUCTION

Fourier-transform infrared spectroscopy (FTIR) is one of the most commonly used techniques for studying clay minerals. Unambiguous assignment of the vibrational bands originating from the stretching modes of adsorbed molecular H₂O (O–H_w) and structural OH (O–H_s) in clay minerals is not always feasible, however. This is especially true for swelling clay minerals such as smectites, which have large water-sorption capacities (*e.g.* Cases *et al.*, 1997; Sato *et al.*, 1992) and may contain significant amounts of adsorbed water under air-dry conditions even upon prolonged drying (*e.g.* Środoń and McCarty, 2008).

New evidence has been presented by Kuligiewicz *et al.* (2015a) that the sharp, high-frequency bands observed at $\sim 3610\text{--}3640\text{ cm}^{-1}$ involve a significant contribution from weakly hydrogen-bonded O–H_w of

adsorbed H₂O molecules. These observations were in agreement with earlier spectroscopic measurements (Russell and Farmer, 1964; Farmer and Russell, 1971; Suquet *et al.*, 1977; Sposito and Prost, 1982; Cariati *et al.*, 1981, 1983; Sposito *et al.*, 1983), and offered the opportunity to obtain layer-charge diagnostics based on the vibrational signature of H₂O in smectite (Kuligiewicz *et al.*, 2015b).

Early computational molecular modeling studies of clays (Skipper *et al.*, 1991; Chang *et al.*, 1995; Boek *et al.*, 1995; Greathouse and Sposito, 1998; Sposito *et al.*, 1999) suggested the existence of H bonds between water and siloxane surfaces. This H bonding implies a specific spatial arrangement of the surface H₂O molecules with respect to oxygen atoms of the basal plane. These MD calculations confirmed the model of Prost (1975) with one

* E-mail address of corresponding author:

ndszczer@cyf-kr.edu.pl

DOI: 10.1346/CCMN.2016.0640409

This paper is published as part of a special issue on the subject of ‘Computational Molecular Modeling.’ Some of the papers were presented during the 2015 Clay Minerals Society–Euroclay Conference held in Edinburgh, UK.

O–H_w bond of the H₂O molecule directed toward the clay surface, donating an H bond to the basal oxygen atom.

The existence of such interfacial H bonding with one O–H_w bond oriented toward the clay surface was later confirmed by simulations of smectites and muscovite (e.g. Wang *et al.*, 2005b, 2009; Marry *et al.*, 2008, 2013; Morrow *et al.*, 2013; Ngouana Wakou and Kalinichev, 2014; Greathouse *et al.*, 2015; Teich-McGoldrick *et al.*, 2015; Zaunbrecher *et al.*, 2015, Loganathan *et al.*, 2016a, 2016b), using more sophisticated force fields specifically optimized for clay–mineral studies, e.g. *CLAYFF* (Cygan *et al.*, 2004). The existence of an additional type of interfacial H₂O located above the ditrigonal cavities of smectites and with both O–H_w bonds directed toward the basal surface was also reported for 2:1 layer silicates of high total layer charge (Wang *et al.*, 2005b, 2009). *Ab initio* calculations showed that these H bonds are relatively short-lived and weaker than typical H₂O⋯H₂O in liquid water (Boek and Sprik, 2003).

In addition, Suzuki and Kawamura (2004) calculated the theoretical FTIR spectra of water adsorbed on Na-beidellite with total layer charge of 0.33 per half unit cell (p.h.u.c.). Based on their modeling, the O–H_w bonds pointing toward the surface of beidellite contribute to a vibrational band at ~3500 cm⁻¹, whereas the O–H_w H bonded to other H₂O molecules produce a band at ~3365 cm⁻¹. The relative intensity of the ~3365–~3500 cm⁻¹ bands increased with increasing water content and for 7 H₂O molecules p.h.u.c. the band at ~3500 cm⁻¹ was no longer detectable.

The experimental and theoretical evidence of the hydrophobic character of the siloxane surface of uncharged clays has been discussed broadly in the literature (e.g. Michot *et al.*, 1994; Bridgeman and Skipper, 1997; Arab *et al.*, 2003; Tunega *et al.*, 2004; Wang *et al.*, 2004, 2005a; Churakov, 2006; Rotenberg *et al.*, 2011; Šolc *et al.*, 2011). For the siloxane surface of charged clays, as for smectites, however, the picture is not as clear. Based on aromatic-hydrocarbon adsorption experiments, this surface was classified by Jaynes and Boyd (1991) as mostly hydrophobic. On the other hand, the neutron scattering technique was used by Sobolev *et al.* (2010) to determine that the surfaces of smectite clays with tetrahedral substitutions are hydrophilic. The importance of the specific structural charge location within a clay layer for the existence of hydrophobic and hydrophilic patches on its surface has also been determined in Monte Carlo computer simulations (Sposito *et al.*, 1999). The relative weakness of the H bonds donated by the interlayer water molecules to the clay basal surface, compared to the typical strength of the H₂O⋯H₂O bonds in bulk liquid water can be considered as a molecular-scale indication of relative hydrophobicity of the smectite siloxane surface.

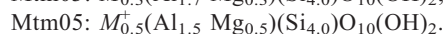
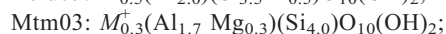
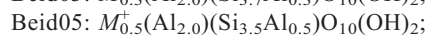
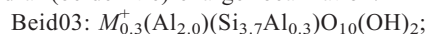
The present study aimed to advance the aforementioned discussion by adding new spectroscopic argu-

ments. Vibrational spectra of interfacial water molecules in several smectites were calculated and analyzed carefully here on the basis of MD simulations in order to identify, interpret, and quantify the variability of the position of the sharp H₂O vibrational band as a function of total clay layer charge, layer-charge localization, and the nature of the interlayer cations, as observed experimentally by Kuligiewicz *et al.* (2015a).

METHODOLOGY

Smectite structures and MD simulations

In order to explore systematically the effects of smectite composition, the type of interlayer cations, and water content on the structure of interlayer H₂O, a series of MD simulations was performed on four models of dioctahedral smectites with a total layer charge of 0.3 or 0.5 p.h.u.c. and octahedral (montmorillonitic) or tetrahedral (beidellitic) charge localization:



The interlayer water content (2.5, 5.0, and 7.5 H₂O p.h.u.c.) and the type of the interlayer cation (Na⁺, Cs⁺, and Ca²⁺) for selected water contents were used as additional variables.

The structural models of the smectites were built on the basis of the pyrophyllite crystal structure (Lee and Guggenheim, 1981), with isomorphic substitutions introduced at specific atomic sites. The Mg/Al ordering in the octahedral sheets was set by maximizing the distance between Mg atoms, following the work of Ortega-Castro *et al.* (2010). The Al/Si ordering in the tetrahedral sheet was random but following the Löwenstein rule, *i.e.* excluding Al–O–Al linkages (Löwenstein, 1954). The simulation supercell was 8 × 4 × 2 unit cells in the *a*, *b*, and *c* crystallographic directions, respectively (~41.6 Å × 36.1 Å × *z* Å; the value of *z* varied in the range of ~12.5–19.0 Å, depending mainly on the amount of water in the interlayer space). The edge surfaces were not considered.

The atoms of the smectite structure were not fixed, *i.e.* they were allowed to move around their crystallographically determined positions according to the modeling force field used. Only one cation in one octahedral sheet was kept frozen in its position in order to keep 2:1 layers in place during the entire simulation span. Partial atomic charges and other interatomic interaction parameters of smectite layers were described using the *CLAYFF* force field (Cygan *et al.*, 2004) with structural OH groups modified by introducing a more accurate Morse potential (Greathouse *et al.*, 2009). Ewald summation was used to calculate the long-range corrections to the electrostatic interactions and the cutoff distance was set at 10.0 Å. Non-electrostatic Lennard-Jones parameters of the interatomic interactions

involving bridging oxygen atoms were modified after Ferrage *et al.* (2011) in order to improve the description of the interlayer water structure of hydrated smectites. The necessity of this modification was justified based on comparisons of experimental and calculated XRD and neutron diffraction data (Ferrage *et al.*, 2011). Unlike the original suggestion of Ferrage *et al.* (2011), however, only the parameters of surface oxygen atoms were modified in the present work, because initial test simulations showed that the modification for all bridging oxygen atoms leads to a substantial and unrealistic deformation of the clay octahedral sheet if the cell volume is not constrained in the simulations at constant pressure, *i.e.* in the *NPT* statistical ensemble (see supplementary information, deposited at <http://www.clays.org/JOURNAL/JournalDeposits.html>). In addition, the Lennard-Jones parameters of tetrahedral Si and tetrahedral Al in the clay structure were also modified to compensate for the increased size of the surface bridging oxygen atoms by applying the usual arithmetic mixing rules for the parameters of interatomic interactions (Table 1).

For a more accurate description of the vibrational properties of water molecules, the parameters of intramolecular interactions for H₂O were taken from the work of Toukan and Rahman (1985) using the implementation proposed by Praprotnik *et al.* (2004). This allowed a more accurate description of the anharmonicity of the O_w–H_w (oxygen and hydrogen of H₂O, respectively) stretching vibrations in the calculated IR spectra in comparison to the simple harmonic vibrational terms of the original *CLAYFF* parameterization (Cygan *et al.*, 2004).

The *NPT*-ensemble MD simulations at constant pressure ($P = 1$ bar) and temperature ($T = 300$ K) were performed for 2.0 ns with the time step of 1 fs, preceded by one temperature annealing cycle from 400 K to 300 K of 0.1 ns. This long equilibration run was

followed by a short 10 ps data-analysis run when atomic positions and velocities were recorded every 2 fs.

Standard periodic boundary conditions were applied (*e.g.* Allen and Tildesley, 1987) and all simulations were performed using the *LAMMPS* molecular modeling program (Plimpton, 1995).

Simulation analysis

The MD-simulated structural data were used to calculate the distributions of angles formed by the dipole axis of interfacial H₂O molecules with respect to a vector normal to the 2:1 surfaces (angle α) as a function of the distance z of O_w perpendicularly to the plane of the basal bridging oxygens (O_b). The direction of the H₂O dipole was defined as a vector from the O_w to the central point between the two hydrogen atoms H_w of the same molecule. As the HOH angle was allowed to vary in the flexible H₂O molecular model used, the methodology introduced some small additional spread of the calculated angles. In addition, the distributions of angles between a given O–H bond of H₂O and a vector normal to the 2:1 surfaces were calculated as a function of the z position (angle β). The position of the plane of basal oxygen atoms was determined by the maximum of the atomic density distribution for these atoms, similarly to the previous studies (Wang *et al.*, 2005b, 2009; Loganathan and Kalinichev, 2013; Szczerba *et al.*, 2014; Ngouana Wakou and Kalinichev, 2014; Greathouse *et al.*, 2015; Teich-McGoldrick *et al.*, 2015; Loganathan *et al.*, 2016a, 2016b). All of these properties were calculated by averaging over the last 1 ns of the equilibrium MD simulation runs.

Calculation of power spectra

The MD-simulated atomic trajectories can be used to calculate so-called ‘power spectra’ (PS) of atomic vibrations that contain an entire distribution of the power (density of states) of all atomic motions in the

Table 1. Parameters of interatomic interactions used in the MD simulations. The modifications compared to the original *CLAYFF* parameters (table 1 in Cygan *et al.*, 2004) are highlighted in bold.

Species	Charge (<i>e</i>)	D_0 (kcal/mol)	R_0 (Å)
Surface bridging O	–1.05000	0.1554	3.8000
Surface bridging O near tetrahedral substitution	–1.16875	0.1554	3.8000
Ordinary bridging O	–1.05000	0.1554	3.5532
Ordinary bridging O near tetrahedral substitution	–1.16875	0.1554	3.5532
Ordinary bridging O near octahedral substitution	–1.18085	0.1554	3.5532
Tetrahedral aluminum	1.57500	$1.8405 \cdot 10^{-6}$	3.4596
Tetrahedral silicon	2.10000	$1.8405 \cdot 10^{-6}$	3.4596
Octahedral aluminum	1.05000	$1.3298 \cdot 10^{-6}$	4.7943
Octahedral magnesium	1.05000	$9.0298 \cdot 10^{-7}$	5.9090
Hydroxyl oxygen	–0.95000	0.1554	3.5532
Hydroxyl hydrogen	0.42500	0.0	0.0
Aqueous sodium ion	1.00000	0.1301	2.6378
Aqueous calcium ion	2.00000	0.1000	3.2237
Aqueous cesium ion	1.00000	0.1000	4.3002

simulated system in a function of vibrations frequency. With certain restrictions, these power spectra can be compared to the experimental vibrational spectra (e.g. Allen and Tildesley, 1987; Kleinhesselink and Wolfsberg, 1992). The power spectra are obtained as Fourier transformations of the so-called velocity autocorrelation function (VACF), which, in turn, can be calculated directly from the MD-simulated dynamic trajectories of the atoms in the modeled system. The frequency of the H₂O stretching vibration is usually well captured by the VACF of the water hydrogen atoms (e.g. Kalinichev, 2001).

In the present study, normalized VACF values based on the last 10 ps period of every MD simulation run were calculated for selected hydrogen atoms with a moving window of 1 ps from the equilibrium part of the MD trajectory recorded every 2 fs:

$$\text{VACF}(t) = \frac{\sum_{f=1}^{n-n_{\text{VACF}}} \sum_{\text{sel.atoms}} \vec{v}_f \cdot \vec{v}_{f+t}}{\sum_{f=1}^{n-n_{\text{VACF}}} \sum_{\text{sel.atoms}} \vec{v}_f \cdot \vec{v}_f} \quad (1)$$

where n is the total number of windows and n_{VACF} is the number of windows used in a particular calculation of VACF; v_f and v_{f+t} are velocities at windows f and $f+t$, respectively. The first sum in the numerator and in the denominator corresponds to averaging over the total number of windows minus the number of VACF windows. The second sum is calculated over all hydrogen atoms of water molecules, or their selected subset based on the distance of the respective H₂O from the clay surface and the angle of H₂O dipole orientation (or angle between one of OH groups of H₂O and a vector normal to the 2:1 surface). The scalar products of instantaneous atomic velocities and their subsequent Fourier transformation into vibrational power spectra were calculated according to standard VACF and PS definitions (e.g. Allen and Tildesley, 1987; Kleinhesselink and Wolfsberg, 1992). For every VACF window, the determination of a H₂O molecule as belonging to a selected position/orientation population was checked at the beginning and at the end of the VACF window. The chosen short duration of the analysis run (10 ps) was, nevertheless, long enough with respect to a typical H-bonding lifetime (0.8–0.9 ps; Kumar *et al.*, 2007), but still short enough not to allow H₂O molecules to change significantly their positions in the interlayer with respect to the clay surface. At the same time, the relatively short time of the individual VACF window (1 ps) is comparable with a typical H-bonding lifetime, but still allows the stretching dynamics of the selected O–H_w bonds to be probed (e.g. Kalinichev, 2001). The choice of both characteristic calculation times ensured that the H-bonding situation of each H₂O molecule was included in a certain selected angle/position subset for VACF calculation.

In order to calculate the power spectra of H₂O vibrations, a cosine Fourier transform of VACF for the water hydrogen atoms was performed as:

$$\text{PS}(\omega) = \sum_{t=1}^{n_{\text{VACF}}} \text{VACF}(t) \cdot \cos\left(\frac{\pi}{n_{\text{VACF}}} \cdot t \cdot \omega\right) \quad (2)$$

The statistical noise was reduced in the first instance by applying a filtering function:

$$\text{VACF}(t) = \text{VACF}(t) \exp(-t/\tau) \quad (3)$$

where τ was set to 0.25 ps.

Due to the normalization of VACF, the intensity of the calculated power spectra can, therefore, be considered as proportional to the total number of H₂O molecules selected for each calculation.

RESULTS AND DISCUSSION

Characteristic features of MD simulations

The composition and adsorbed water content of all simulated clay models are presented in Table 2 along with the resulting basal spacings. The 2W model for Cs-smectite is purely hypothetical and does not correspond to any experimental or natural conditions (e.g. Ngouana Wakou and Kalinichev, 2014).

The values of the calculated basal spacings match closely those obtained by modeling the experimental X-ray diffraction (XRD) patterns: $d_{001_1w} = 11.6\text{--}12.9 \text{ \AA}$, $d_{001_2w} = 14.9\text{--}15.7 \text{ \AA}$, and $d_{001_3w} = 18\text{--}19 \text{ \AA}$ (e.g. Dazas *et al.*, 2015). The data show clearly that for the same water content and interlayer cation (Na⁺) the basal spacing, d_{001} decreases with increasing layer charge (e.g. 15.95 Å for Mtm03Na_2W and 15.37 Å for Mtm05Na_2W). This trend is in agreement with data from the literature (e.g. Sato *et al.*, 1992; Ferrage *et al.*, 2005, 2007), whereas some variation is related also to the layer charge location. Substantial differences in basal spacings were also observed as a result of the replacement of interlayer cations from Na⁺ or Ca²⁺ to Cs⁺ (e.g. 15.37 Å for Mtm05Na_2W, 15.38 Å for Mtm05Ca_2W and 16.14 Å for Mtm05Cs_2W). These differences were caused mainly by the increased size of the cation and by differences in hydration energies.

In agreement with other recent simulations (e.g. Wang *et al.*, 2005b, 2009; Morrow *et al.*, 2013; Ngouana Wakou and Kalinichev, 2014; Greathouse *et al.*, 2015; Teich-McGoldrick *et al.*, 2015; Zaunbrecher *et al.*, 2015; Loganathan *et al.*, 2016a, 2016b), a typical snapshot of the interlayer structure (Figure 1) shows that H₂O molecules close to the siloxane surface tend to be specifically oriented. Within a distance of <3.5 Å between O_w and the siloxane surface two such preferred orientations could be distinguished. The population closer to the surface corresponds to H₂O with both O–H_w bonds pointing toward the surface (bidentate), whereas a more distant and more pronounced population is due to the H₂O

Table 2. Interlayer cation and water content of the simulated clay models and the resulting basal spacing.

Model	$n(\text{H}_2\text{O})$ p.h.u.c.	$n(\text{H}_2\text{O})/n(\text{M}^{\text{m}+})$	H_2O (wt.%) normalized to the total mass (smectite + H_2O)	H_2O (wt.%) normalized to dry mass (smectite)	Calculated d_{001} (Å)*
Beid03Na_1W	2.5	8.333	10.93	12.28	12.99
Beid03Na_2W	5	16.667	19.71	24.55	15.94
Beid03Na_3W	7.5	25.0	26.92	36.83	18.88
Beid05Na_1W	2.5	5.0	10.82	12.13	12.76
Beid05Na_2W	5.0	10.0	19.53	24.26	15.38
Beid05Na_3W	7.5	15.0	26.68	36.39	18.34
Mtm03Na_1W	2.5	8.333	10.95	12.29	12.86
Mtm03Na_2W	5.0	16.667	19.73	24.58	15.95
Mtm03Na_3W	7.5	25.0	26.94	36.88	18.95
Mtm05Na_1W	2.5	5.0	10.84	12.16	12.58
Mtm05Na_2W	5.0	10.0	19.56	24.31	15.37
Mtm05Na_3W	7.5	15.0	26.72	36.47	18.14
Beid03Ca_2W	5.0	33.334	19.75	24.61	15.82
Beid05Ca_2W	5.0	20.0	19.59	24.36	15.38
Mtm03Ca_2W	5.0	33.334	19.77	24.64	15.95
Mtm05Ca_2W	5.0	20.0	19.62	24.41	15.38
Beid03Cs_2W	5.0	16.667	18.39	22.53	16.34
Beid05Cs_2W	5.0	10.0	17.45	21.13	16.13
Mtm03Cs_2W	5.0	16.667	18.40	22.55	16.41
Mtm05Cs_2W	5.0	10.0	17.47	21.17	16.14

* Standard deviation is $\sim\pm 0.05$ Å.

pointing only one of its O–H_w bonds toward the surface and the second one toward the bulk of the interlayer (monodentate). In order to quantify these differences,

these two populations were investigated as a function of smectite charge, type of the interlayer cations, and the degree of hydration of the interlayer space.

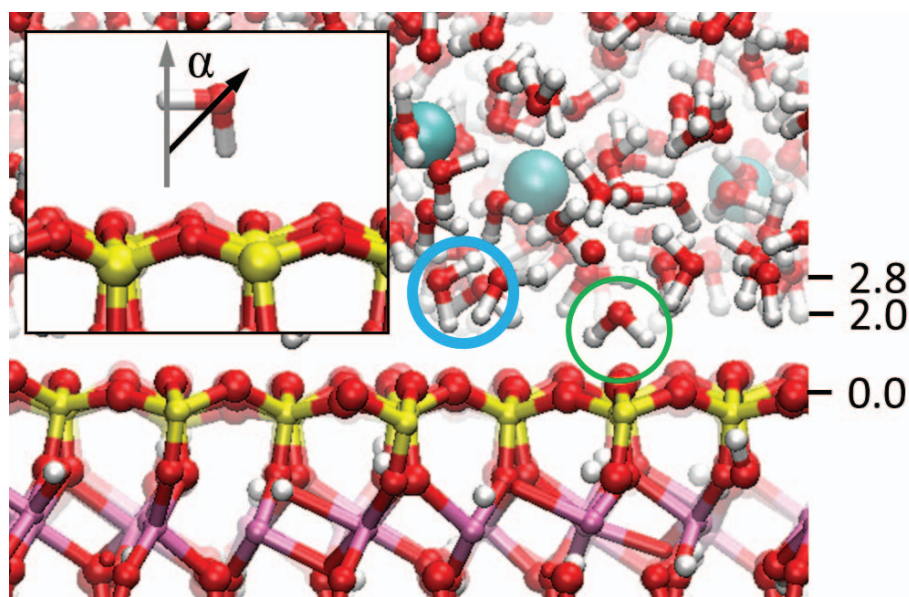


Figure 1. Snapshot of part of the MD simulation cell for Mtm05Na_3W. H_2O closer to the layer surface is oriented with two O–H_w bonds pointing to the surface (thin green circle), whereas H_2O further from the surface has one O–H_w bond oriented toward the surface (thick blue circle). The inset shows the definition of the angle α formed by the H_2O dipole vector and the surface normal. The vertical scale (Å) shows the average distance in the z direction relative to the oxygens of the basal plane.

Position of the cations in the interlayer space

The distribution of interlayer cations for different smectites (solid blue lines in Figures 2 and 3) exhibited a clear dependence on the amount and location of layer charge, as well as on the type of the cation. In the case of 1W sodium smectites, two separate maxima were visible, each corresponding to inner-sphere coordination of H₂O to the surface. For 2W sodium structures, a

strong tendency to form a third maximum corresponding to fully hydrated cations (outer sphere) in the middle of the interlayer was observed. The ratio between the central and side (inner sphere) cation distributions depended on the charge location, whereas changes in total charge had a similar effect on both of these maxima. This result is in agreement with other recent simulations and is supported by calculated XRD data (Dazas *et al.*, 2015; Teich-McGoldrick *et al.*, 2015). In

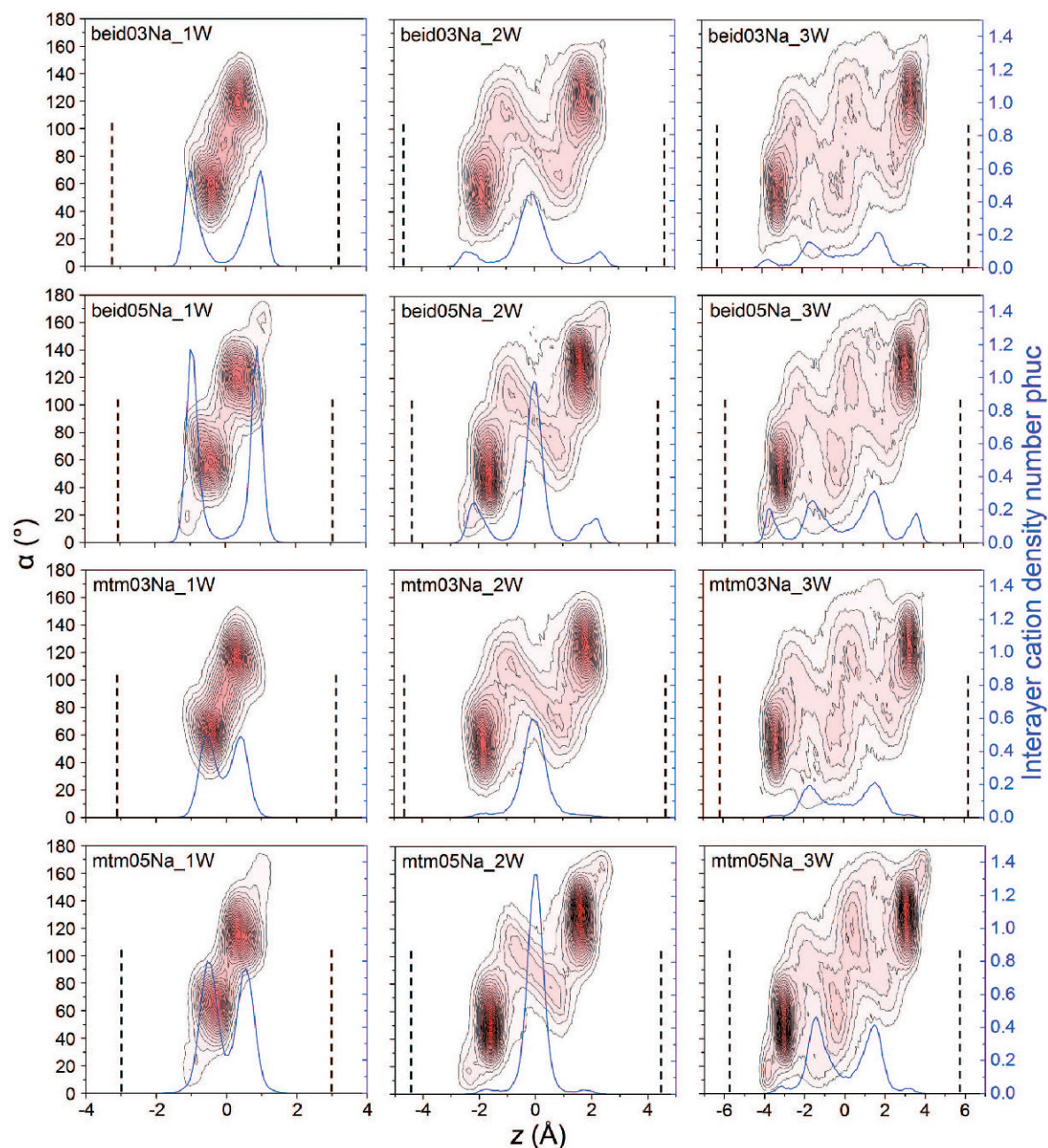


Figure 2. Dependence of the H₂O dipole vector orientation contours (see Figure 1 for the definition of α) on the z position for various hydration levels of different Na⁺-smectites. The interlayer distribution of the cations is shown by solid blue lines. Dashed lines indicate the location of the surface (basal oxygen positions).

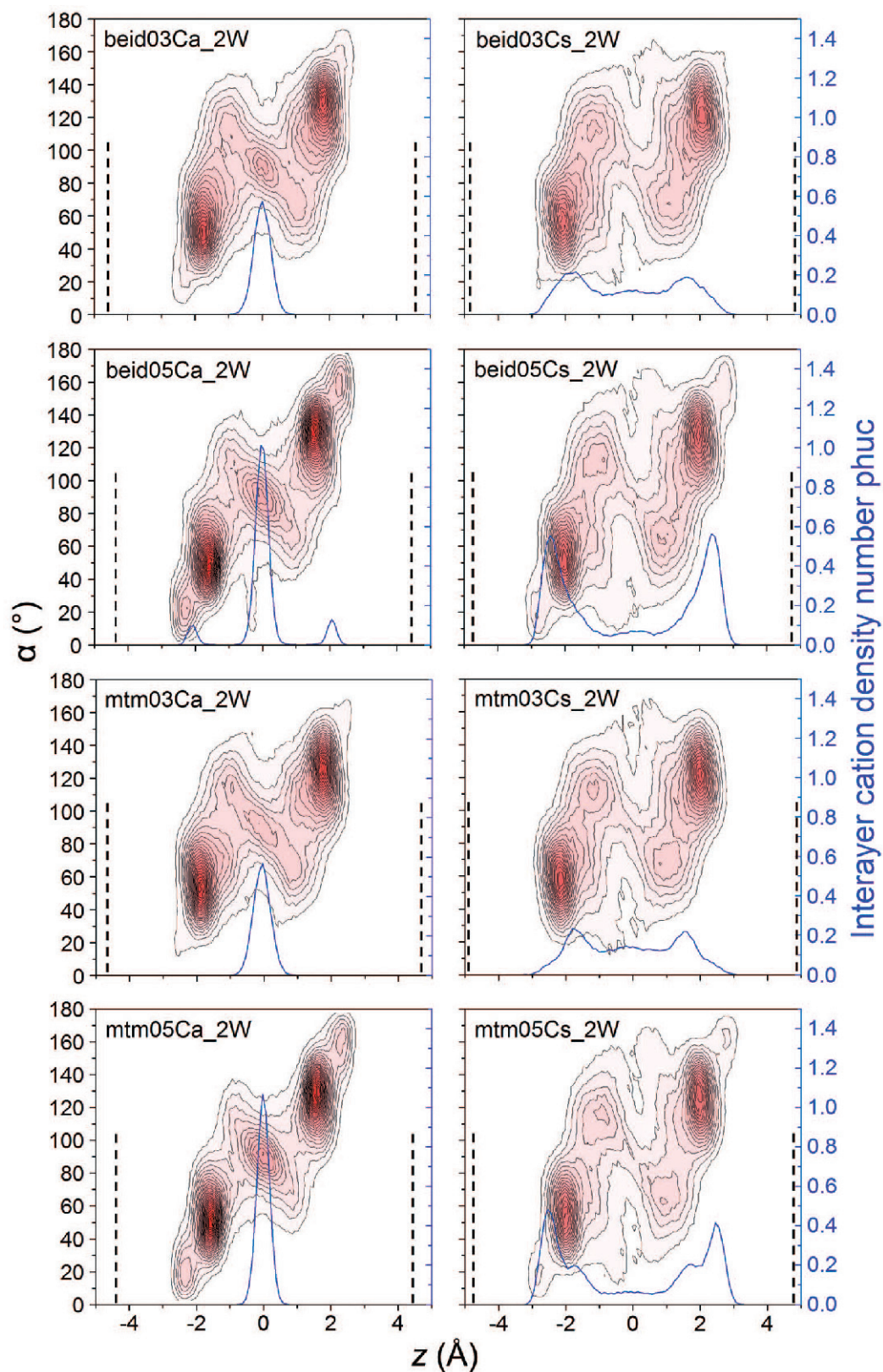


Figure 3. Dependence of the H₂O dipole orientation contours on the z position for 2W hydration level of Ca²⁺- and Cs⁺-smectites. Symbols as in Figure 2.

the case of 3W structures, outer-sphere Na^+ ions formed two maxima close to the interlayer center instead of one as in 2W. The data for the Mtm03Na_3W structure were very similar to the results presented by Dazas *et al.* (2014). With increasing tetrahedral charge, a tendency to form more inner-sphere complexes with the siloxane surface was observed.

The effect of changing the interlayer cation from Na^+ to Ca^{2+} was investigated for the models with 2W hydration. Comparison of smectites in Ca^{2+} form (Figure 3) with those in Na^+ form (Figure 2) indicated that, despite the two-fold increase in the cation hydration enthalpy, the only effect was the vanishing of the (already weak) population of cations in the vicinity of the surface. The only exception was Beid05Ca_2W, for which some remaining contribution of ions forming inner-sphere complexes was observed.

On the other hand, the lowest hydration enthalpy Cs^+ ions had a tendency to remain close to the surface (Figure 3), which is in excellent agreement with other recent Cs^+ -smectite simulations (Ngouana Wakou and Kalinichev, 2014; Teich-McGoldrich *et al.*, 2015; Zaunbrecher *et al.*, 2015; Loganathan *et al.*, 2016a). The distribution of Cs^+ in the interlayer was substantially different from those of Na^+ and Ca^{2+} , which were generally quite similar to each other (compare Figures 2 and 3).

H₂O orientation

The contour maps of the angular distributions of the interlayer H_2O dipole vectors with respect to the direction normal to the surface (α angle), plotted as a function of the z position (Figure 2), enabled the distinction of the two preferred surface-oriented types of water molecules marked in Figure 1. The predominantly bidentate population was located closer to the surface at a distance of ~ 2.0 Å from the surface and $\alpha \approx 0$ – 30° , similar to ideal theoretical values (observed in smectites with charge of 0.5 p.h.u.c.). A more distant and more pronounced monodentate population was at distances from the surface of ≈ 2.8 Å and oriented in a broad range of angles between 30 and 80° with a maximum at $\alpha \approx 55^\circ$, which matches the ideal theoretical value for one OH vector pointing perpendicularly to the smectite surface (half of the 105° angle of H_2O). For greater hydration levels, a third population of water molecules was observed closer to the middle of the interlayer. The orientational distribution of this population depended significantly on both the hydration level of the specific smectite and the type of the interlayer cation. The latter dependence was observed clearly when comparing the distribution in Mtm05 for the same hydration levels but different interlayer cations (Figures 2 and 3).

The presence of monodentate H_2O was ubiquitous. This sub-population was abundantly visible for all smectites, all cations, and all hydration levels. A

noticeable dependence of the location of the distribution maxima was observed, however: greater average H_2O dipole vector angles were observed for low-charge smectites, for lower hydration levels, and for Cs^+ as the interlayer cation.

The bidentate H_2O population was far less abundant, could be detected only in high-charge smectites, and was practically absent from their low-charge analogs. Layer charge increasing beyond 0.5 p.h.u.c. is, therefore, expected to increase further the amount of bidentate molecules, predicting its high contribution at charges approaching 1 p.h.u.c. (mica, vermiculite), which was indeed reported by Wang *et al.* (2005b, 2009) and Loganathan and Kalinichev (2013) for muscovite. Furthermore, in all smectites studied, a dependence of the bidentate H_2O population on hydration level was observed: for a given smectite, the relative number of bidentate H_2O decreases upon drying.

The H_2O orientation also depends on the type of the interlayer cation. As the majority of Cs^+ cations are located close to the smectite surface, a noticeable decrease of bidentate H_2O population in Cs^+ -smectites in comparison to their Na^+ - and Ca^{2+} -analogs was observed. This effect was, however, small compared to the dependence of the bidentate population on layer charge. A noticeable decrease in the maximum amplitude corresponding to monodentate population was also observed for the Cs^+ form. This decrease was accompanied by the transfer of H_2O to the middle of the interlayer.

Vibrational spectra of H₂O in the smectite interlayer

The sharp, high-frequency IR band originating from adsorbed water at ~ 3615 cm^{-1} (in H_2O form) and ~ 2685 cm^{-1} (in D_2O form) is a common feature for all hydrated smectites (Kuligiewicz *et al.*, 2015a, 2015b). Its intensity depended very little on the degree of clay hydration over a broad range of relative humidity, and its frequency exhibited a weak but systematic decrease (red-shift) upon increasing the total layer charge, with no measurable dependence on charge location. For a given layer charge, the dependence of the peak position on the field strength of the interlayer cation for high hydration enthalpy cations (Na^+ , Ca^{2+} , Mg^{2+}) was negligible and only low hydration cations (Cs^+ , K^+) could be distinguished. These trends were the opposite of what was observed for the main O–H_w (O–D_w) stretching envelopes, located at ~ 3400 cm^{-1} (~ 2500 cm^{-1}). The latter envelopes were known to exhibit a strong dependence of their intensity on hydration level and their position on interlayer cation, but were relatively unaffected by the smectite layer charge or charge localization (*e.g.* Xu *et al.*, 2000; Madejová *et al.*, 2002; Kuligiewicz *et al.*, 2015a, 2015b).

Thus, the sharp, high-frequency IR band observed in water vapor-saturated smectites was attributed to a mechanism that must be common to all smectites at

high hydration levels, regardless of interlayer cation. In addition, the high-frequency band must account for H-bonding interactions that are considerably weaker than those encountered in bulk H₂O or aqueous solutions of common salts, and its exact position ought to show a measurable dependence on the total charge of the 2:1 layer (Kuligiewicz *et al.*, 2015a, 2015b).

In order to provide a quantitative explanation for the aforementioned experimental phenomena, the power spectra for hydrogen atoms of interlayer H₂O molecules were calculated for different smectites and compared to the spectrum of pure bulk water, the latter calculated with the same molecular model (Figure 4).

The results showed that water in smectites exhibits a considerable increase in its spectral density at higher frequencies (~3600–3800 cm⁻¹) with respect to a bulk-water spectrum. The simulated spectrum of bulk water, however, shows some excessive high-frequency spectral density around 3730 cm⁻¹, which is not observed experimentally, and indicates some limitations of the present model. Nevertheless, the shape of the power spectrum of bulk water agrees perfectly well with the spectrum obtained earlier by the same methodology (Tay and Bresme, 2006) and still represents one of the most accurate models describing the dynamics of O_w–H_w stretching vibrations in water (*e.g.* Kalinichev, 2001; Guillot, 2002). In addition, the calculated results do not show the low-frequency band at ~3250 cm⁻¹, which has been found in experimental data and thus is consistent with an assignment of this band to Fermi resonance (Efimov and Naberukhin, 2002; Sovago *et al.*, 2009).

Power spectra were also calculated for four different smectites with varying amounts of adsorbed water: Beid03Na, Beid05Na, Mtm03Na, and Mtm05Na (Figure 5). The results showed that with increasing numbers of H₂O molecules in the smectite interlayer, the relative intensity of the lower-frequency peak at ~3500 cm⁻¹ increased. This was in qualitative agreement with the experimental observations of Kuligiewicz *et al.* (2015a), who reported that the higher-frequency peak is nearly fixed and the intensity of the lower-frequency peak varies significantly with water content. In the present study, the peak intensity at ~3750 cm⁻¹ depended on hydration, but this may, to some extent, be related to the limitations of the specific H₂O molecular models used.

In order to further analyze the influence of different factors on the higher-frequency band, its positions were determined by fitting procedures. The low-frequency band was fitted with a mixed Gaussian-Lorentzian function (percentage of Lorentz function was optimized), while the higher-frequency function was fitted with a simple Gaussian function. In addition, a small combination band at ~4000 cm⁻¹ was fitted with another Gaussian (Figure 6).

Increasing the smectite total layer charge induced a noticeable red-shift of the high-frequency peak, in

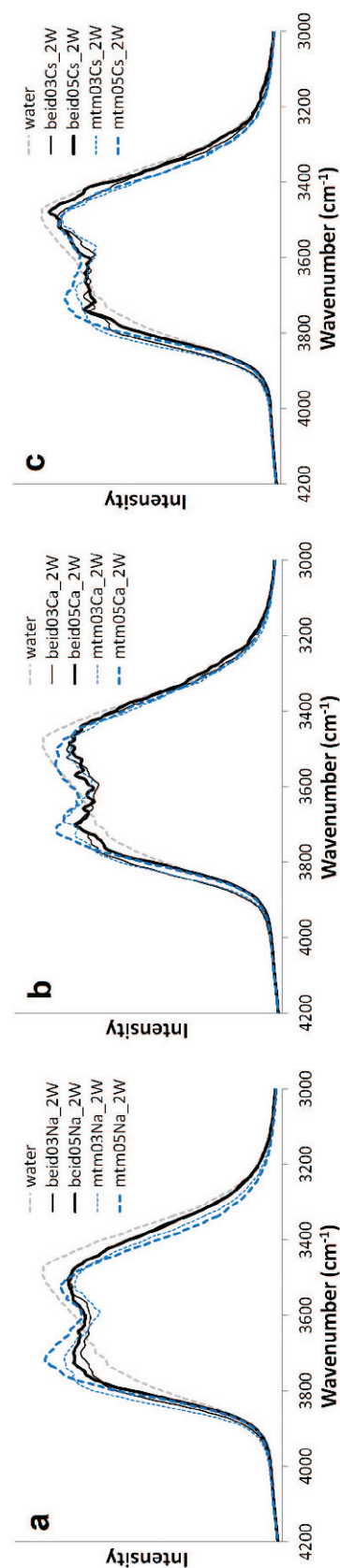


Figure 4. Power spectra for hydrogens of interlayer H₂O in smectites with two hydration layers (2W) in the O–H_w stretching range showing the effect of the total layer charge and the cation-dependence: (a) Na⁺ form; (b) Ca²⁺ form; (c) Cs⁺ form. Increase of the spectral density at higher frequency is clearly visible in comparison with the spectrum of bulk water.

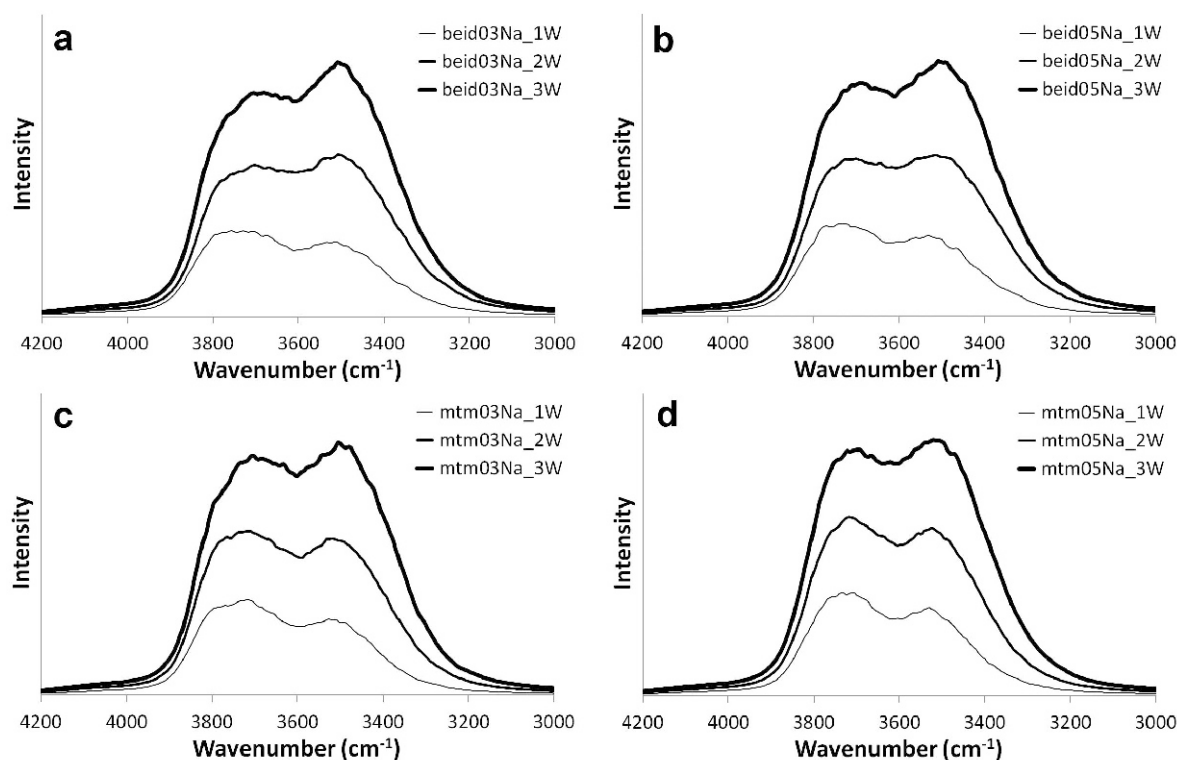


Figure 5. Power spectra for hydrogens of interlayer H₂O in the O–H_w stretching range for Na⁺-beidellites (upper) and Na⁺-montmorillonites (lower) with different total layer charge and different water contents. The spectra were scaled by their H₂O content.

remarkable agreement with experimental data (Kuligiewicz *et al.*, 2015b). This shift was observed in Na⁺ montmorillonites and beidellites at any hydration level (Figure 7a) and also in the 2W forms for any cation (Figure 7b). Only one exception was found: Mtm05Na_3W exhibited higher frequency for the sharp peak than Mtm03Na_3W. Contrary to the experimental observations (Kuligiewicz *et al.*, 2015a), the position of the high-frequency peak was found to depend on charge location and water content.

In addition, the MD results showed a substantial difference in peak position between the Na⁺ and Ca²⁺ forms of smectites (Figure 7b), which are not visible experimentally (Figure 7c, Kuligiewicz *et al.*, 2015a). Peak positions of the Cs⁺ forms also exhibited trends in relation to Na⁺ and Ca²⁺ forms that are different in MD compared to the experiment.

These discrepancies between the experimental trends and the outcomes of MD simulations may be related to the approximations involved in the latter, primarily in certain features of the CLAYFF model (Cygan *et al.*, 2004). The Lennard-Jones parameters of Ferrage *et al.* (2011) should be optimized more accurately, the hexagonal cavity in the tetrahedral sheet ought to have lower ditrigonal symmetry. A better description of the structure would affect the distribution and orientation of H₂O. The model for H₂O may also have limitations and

the power spectra have excessive high-frequency spectral density at 3728 cm⁻¹. Finally, uncertainties introduced by the fitting procedure can be observed (Figure 6). In spite of all these limitations, the overall picture is relatively consistent: all the smectites studied exhibit a stretching band at lower frequencies and this band shifts to lower energy upon increasing layer charge (Figure 7a,b).

Molecular origin of the sharp O–D_w/O–H_w band

Calculations of the power spectra of specific sub-sets of interlayer water hydrogen atoms were performed in order to explain in more detail which part of the surface H₂O population is responsible for the sharp, high-frequency vibrational band observed in the experimental spectra (Kuligiewicz *et al.*, 2015a). Each subset was defined by a common range of distances from the surface, along direction *z*, and H₂O dipole orientation angle, α (Figure 1). A H₂O molecule belongs to a certain sub-set if it is found within the same (*z*, α) range in both the first and the last time-window of the VACF calculation. The results for three representative smectites (Mtm03Na_2W, Beid03Na_2W, and Mtm05Ca_2W) are presented in Figure 8. Spectral intensities were scaled by the number of H₂O molecules identified in each subset in order to compare the contribution of each subset to the total spectrum.

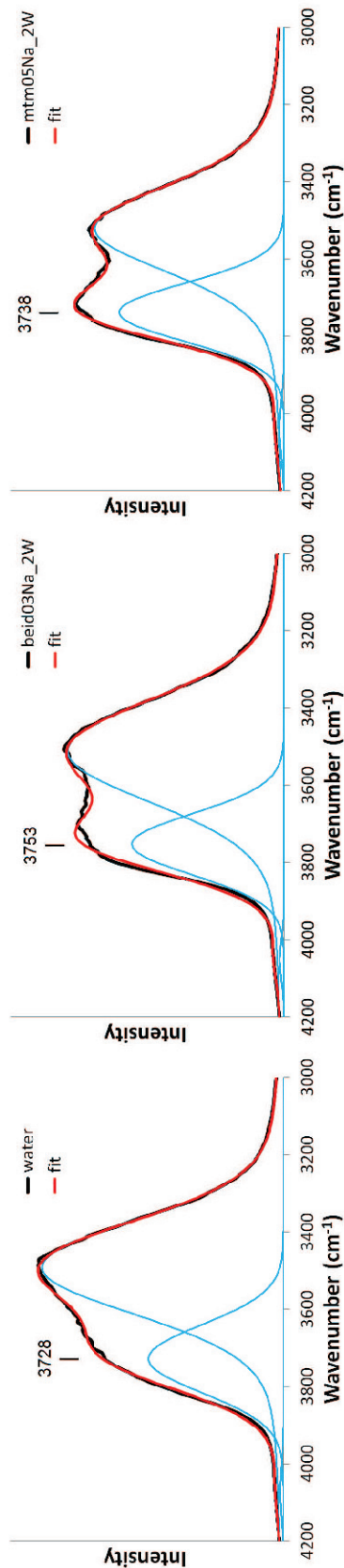


Figure 6. Deconvolution of power spectra of pure water and two representative smectites.

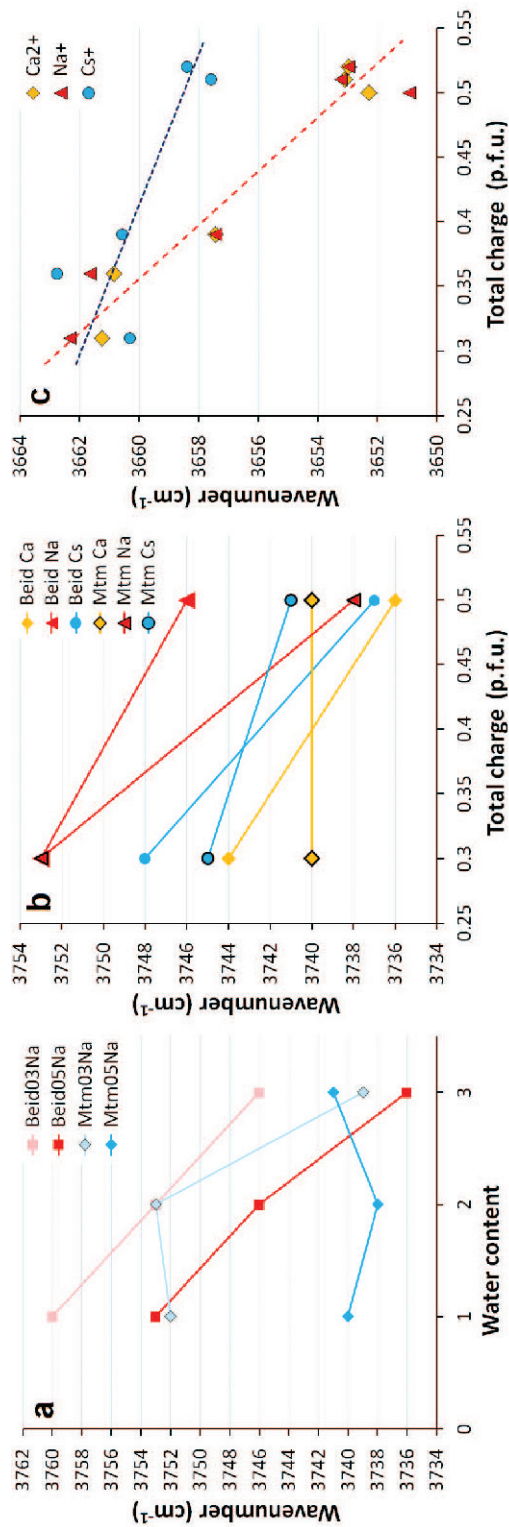


Figure 7. Comparison of frequencies: (a) dependence on water content for Na⁺-smectites in MD; (b) dependence on interlayer cation for 2W forms in MD; in comparison to (c) results from Kuligiewicz *et al.* (2015a). To obtain frequencies for H₂O, the experimental values for D₂O were scaled by × 1.36.

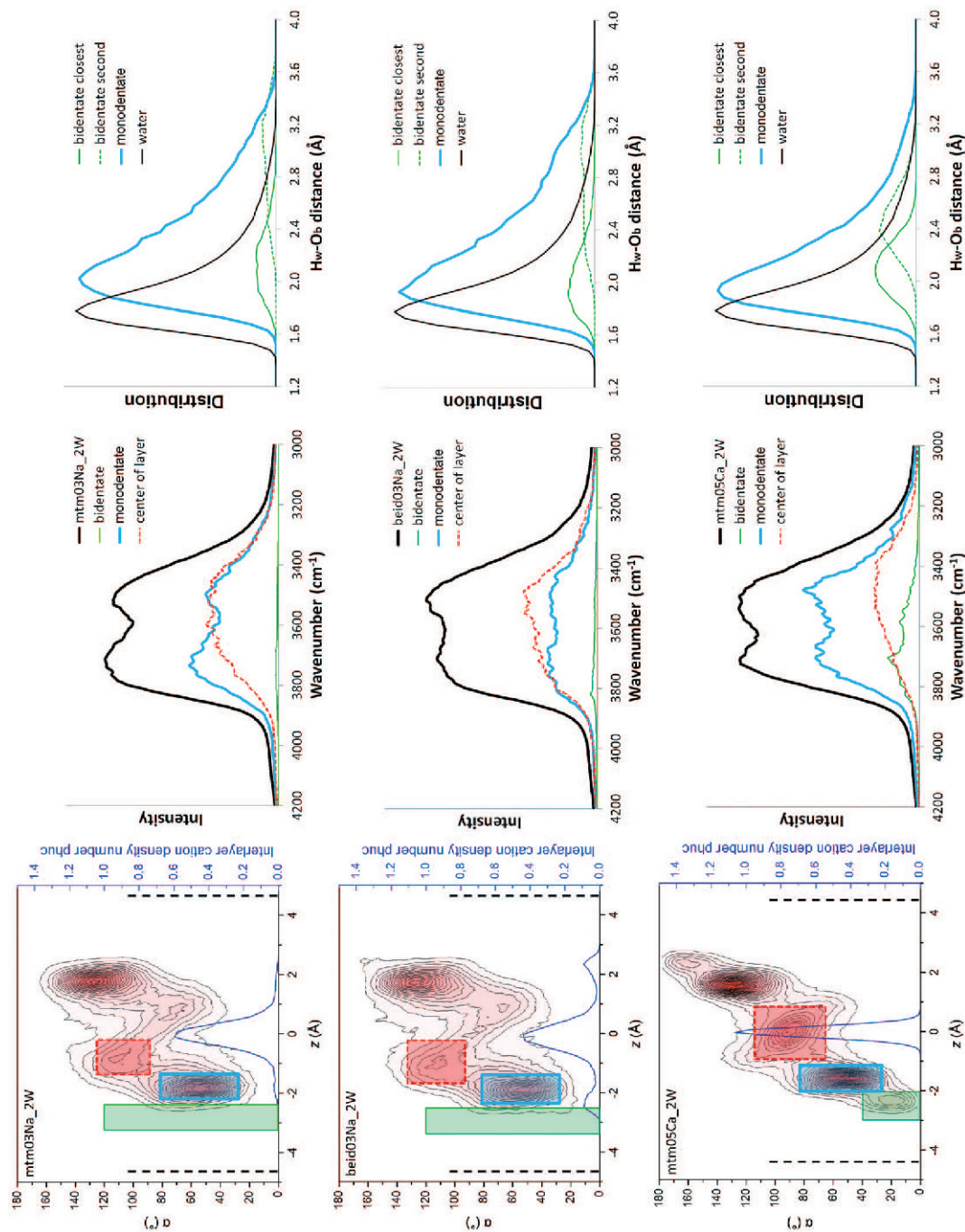


Figure 8. H₂O dipole orientation with respect to the surface normal for selected sub-sets of water molecules having their z and α values within the marked ranges (left) and power spectra of O–H_w stretching vibrations calculated for each individual sub-set (center): thin green – bidentate population, thick blue – monodentate population, dashed red – water in the center of interlayer. Right column – the distributions of the shortest H-bonding distances of interfacial H₂O molecules with basal oxygens (O–H_w···O_b) in the bidentate and monodentate orientations, compared to distribution of O–H_w···O_w distances in pure water.

This analysis demonstrates that H₂O molecules at the center of the interlayer are not responsible for producing the sharp spectral feature. The latter originates instead from the overlapping contributions of both monodentate and bidentate orientations of surface H₂O. The contribution of the monodentate orientation is, however, much stronger because of the greater number of H₂O molecules populating this sub-set. If present, bidentate H₂O gives a very small, though non-negligible, contribution to the power spectrum at frequencies that are, on average, greater than those of the monodentate population.

Based on the correlation of IR frequency of the O–H stretching band and the length of the H bond, O–H_w···O, (Libovitzky, 1999), a peak at ~3600 cm⁻¹ may correspond to an O–H_w···O distance >2.2 Å (*i.e.* an O_w···O distance >3.2 Å), and indicates a relatively weak H bond donated to the surface (*e.g.* Kalinichev, 2001; Kumar *et al.*, 2007). In order to obtain deeper insight into the studied problem, the distribution of the shortest O_w–H_w···O_b distances in the monodentate and bidentate sub-sets were calculated, therefore (Figure 8, right column). The results showed a relatively broad distribution of the distances, with the maximum for monodentate H₂O at ~1.9 Å for Beid03_Na and Mtm05Ca_2W, and ~2.0 Å for Mtm03Na_2W. For comparison, in bulk liquid water the maximum of the shortest O–H_w···O_w distance is at ~1.8 Å (*e.g.* Kalinichev, 2001; Kumar *et al.*, 2007). The weighted average of the calculated O–H_w···O_b distributions is, however, a little greater than the maxima: 2.24 Å for Beid03_Na, 2.16 Å for Mtm05Ca_2W, and 2.27 Å for Mtm03Na_2W, compared to 1.95 Å in bulk water. In bulk water a contribution of H bond distances >2.2 Å was observed, but this is much smaller than for smectites. Low-charge smectites exhibited a significantly larger contribution of weak H bonds. For the high-charge smectite Mtm05Ca_2W, the contribution of weak H bonds due to H₂O molecules in monodentate orientation was noticeably smaller. This explains the higher frequency and intensity of the high-frequency monodentate peak in the vibrational spectrum of this smectite. In the case of the bidentate population, one of the O–H_w···O_b distances had a maximum also at ~1.9–2.0 Å, resulting in a H bond of a comparable strength, while the second one was significantly longer and weaker. This analysis suggests that upon increasing the total layer charge, the H-bond distances of the bidentate sub-set are decreasing and cause the red-shift of the calculated power spectrum.

Due to its ubiquitous presence and relative abundance, the population of monodentate surface H₂O is mainly responsible for the presence of the sharp, high-frequency OH-stretching feature observed in experiments (Kuligiewicz *et al.*, 2015a). This is in very good agreement with previous experimental data (*e.g.* Russell and Farmer, 1964; Farmer and Russell, 1971; Prost,

1975; Suquet *et al.*, 1977; Sposito and Prost, 1982; Sposito *et al.*, 1983) which linked the high-frequency band to H₂O at the surface of the interlayer, pointing one of their O–H_w bonds toward the siloxane surface. In certain cases the bidentate sub-population may provide a non-negligible contribution, as observed for higher-charged smectites, *e.g.* for Mtm05_Ca_2W.

Possible alternative molecular mechanisms responsible for the sharp O–Dw/O–Hw band

Evidence from MD simulations in support of the experimental data, suggested that the sharp, high-frequency band in the IR spectra of hydrated smectite clearly originates from H₂O molecules oriented toward the clay surface. Can there be any other contribution to this sharp IR band? One possibility that would also be linked to surface H₂O, could, for example, involve the second O–H_w bond of monodentate H₂O, *i.e.* that oriented toward the middle of the interlayer, away from the siloxane surface. As the surface H₂O molecules have relatively fixed orientations, their O–H_w bonds that are pointing away from the surface might have a decreased number of available H-bond acceptors within a suitable range and orientation around them. Such a lower coordination could, in principle, contribute in part to the observed sharp, high-frequency IR band. To examine this possibility, the subsets representing two separate hydroxyls of the monodentate population in Mtm05Ca_2W and Mtm05Na_2W were investigated (Figure 9).

In the case of monodentate H₂O, one H bond is donated to the surface (thick blue rectangle in Figure 9), while the second is donated to another H₂O (dashed orange rectangle in Figure 9). The corresponding power spectra show that only the hydrogens oriented toward the surface contribute to the high-frequency band. The power spectrum of the second hydrogen resembles that of bulk water, with even a slightly greater intensity of the vibrational band at lower frequency of ~3500 cm⁻¹, indicating a relatively strong H bonding to other interlayer H₂O molecules. This is also confirmed by comparison of the shortest O–H_w···O_w distances of this sub-population and the corresponding distances in pure water (right column in Figure 9). The two distributions are practically identical.

A second mechanism potentially responsible for the emergence of the high-frequency H₂O stretching band could be related to the influence of interlayer cations. The latter could deform the H bonding structure of H₂O molecules around them and possibly induce some H-bond breaking. Clear evidence against this possibility is given in Figure 8: H₂O molecules in the middle of the interlayer (red rectangle) were found not to contribute to the high-frequency band of interest. This is especially obvious in the case of Mtm05Ca_2W, where H₂O molecules in the hydration shell of Ca²⁺ are oriented around the ions exactly in the center of the interlayer.

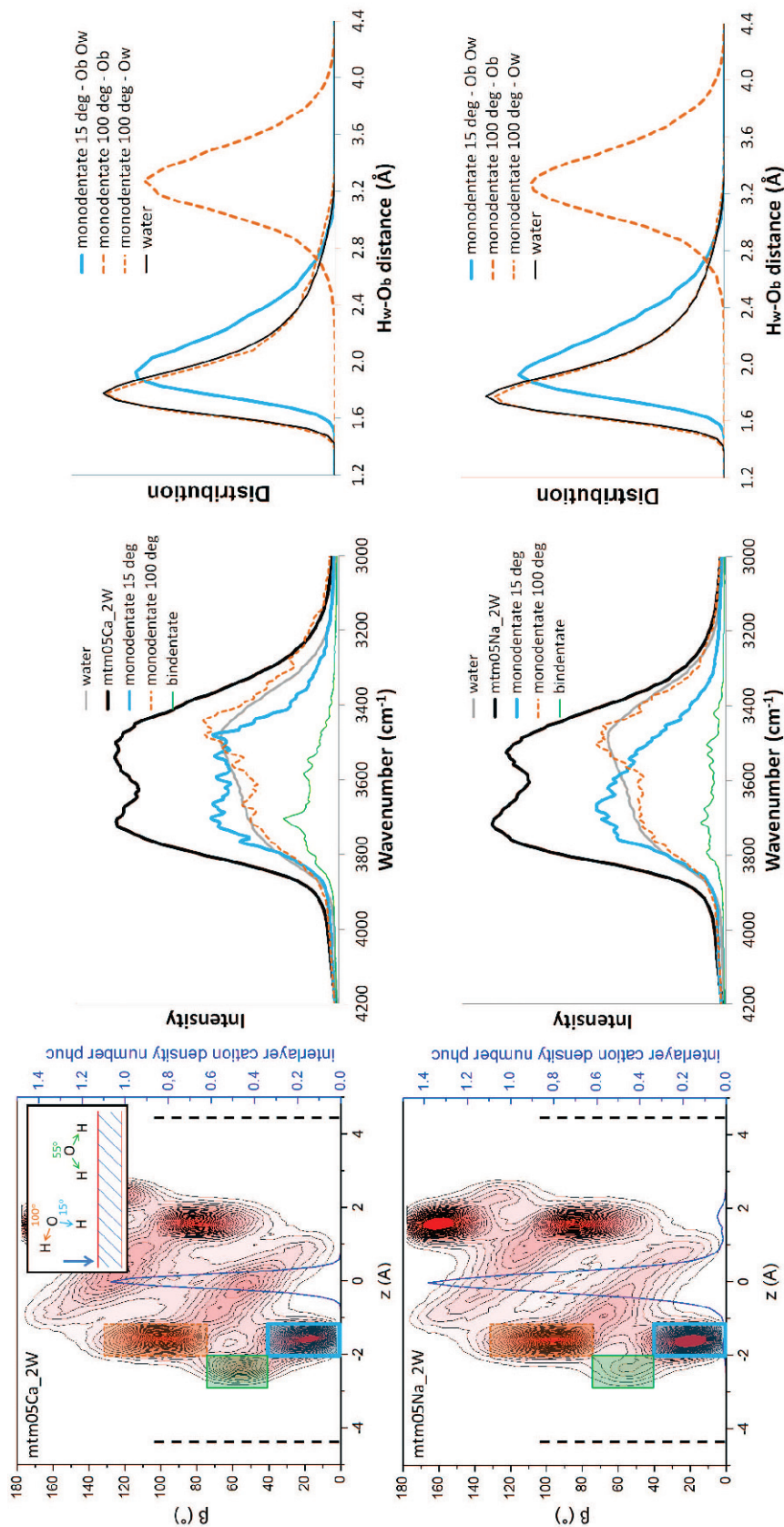


Figure 9. Orientation of the O–H_w vector of interfacial H₂O with respect to the surface normal (β) at various distances, along direction z, from the basal surface of Mtm05Ca_2W and Mtm05Na_2W smectites (left). Calculated power spectra for the sub-sets of H₂O molecules (color marked for the selected β and z ranges) are shown in the center. Right: the distributions of the shortest H-bonding distances of monodentate H₂O with the basal oxygens (O_w–H_w...O_b) and/or other oxygen (O_w–H_w...O_w), compared to distribution of O_w...O_w distances in pure water. Thin green – bidentate population, thick blue – water O–H_w bond oriented toward the surface, dashed orange – O–H_w bond oriented toward the interlayer. Power spectra were scaled by the number of H₂O molecules.

Hydrogen bonding in the interlayer space of smectite

The question regarding other possible molecular mechanisms responsible for the sharp high-frequency $O-D_w/O-H_w$ band can be expressed alternatively as follows: does interlayer water contain a sub-population of H_2O molecules for which the $O-H_w\cdots O$ distance of donated H bonds is $>\sim 2.2$ Å (Libovitzky, 1999)? Obviously, the results of this analysis are only valid in comparison to those for pure bulk liquid water, due to the method, artificial, non-negligible contribution of weak H bonds in the latter (see Figures 8 and 9).

To address this question, the numbers of accepted and donated H bonds were calculated depending on the distance along direction z of the H_2O molecules involved from the smectite siloxane surface. In the ordered ice structure, each H_2O donates two strong H bonds to other H_2O and also accepts two strong H bonds from two other H_2O molecules. In liquid water, the number of donating and accepting H bonds formed by each H_2O molecule is somewhat smaller than in ice due to the molecular disorder, and depends on temperature, density, and other thermodynamic factors. The exact number of H bonds experienced by a H_2O molecule in each situation also depends to some extent on the assumed criterion used in H-bonding calculations (*e.g.* Kalinichev, 2001; Kumar *et al.*, 2007).

A geometric definition for counting H bonds (HB) was adopted from the literature (Wang *et al.*, 2009; Loganathan and Kalinichev, 2013). According to this definition, an H bond is assumed to exist if the $H\cdots O$ distance between the donor and acceptor is <2.45 Å and the angle between the $O-H$ and $O\cdots O$ vectors is $<30^\circ$. A systematic application of this criterion enabled the quantitative visualization of the general H bonding trends of interlayer H_2O molecules for several model smectites (Figure 10). As expected, H bonds donated to surface O_b atoms from both bidentate and monodentate H_2O populations were identified in all cases (thick solid lines in Figure 10). The maximum of their distribution corresponded to the monodentate population, whereas the small shoulder closer to the surface originated from bidentate H_2O . Besides donating to the basal surface, both bidentate and monodentate H_2O accepted H bonds from and donated to other H_2O in the interlayer (dashed and thin solid lines, respectively, in Figure 10). The maxima of the accepted and donated H-bonding distributions corresponded clearly to the expected (*e.g.* Ferrage *et al.*, 2011; Nguouana Wakou and Kalinichev, 2014) twin maxima of the O_w distribution along z , shown previously for all 2W structures (Figures 2 and 3). Subtler differences in the fractions of accepting and donating H bonds depended on the charge and the type of the interlayer cation (Figure 10).

The distributions of H bonds along z (Figure 10) provide a general picture of the H bonding structure in smectite interlayers, but they do not indicate directly the

locations of particularly weak hydrogen bonds. To address this issue, the distributions of H bonds on the basis of their strength was also calculated (Figure 11). This was achieved by modifying the aforementioned geometric definition of the H bond to probe only the relatively weak interactions having $O-H_w\cdots O$ distances in the range $2.2-2.7$ Å and compare such a subset of the H-bond distribution to the original definition ($O-H_w\cdots O$ distance <2.45 Å). In both cases the $H_w-O\cdots O$ angle was kept $<30^\circ$. The plots in Figure 11 show only the average distributions of H bonds experienced by each H_2O molecule, and therefore do not inform the absolute contributions of each molecular orientation to the final spectra.

For the general case where all possible H bonds in the system are considered (Figure 11a), the number of accepted H bonds per H_2O molecule was relatively constant with little dependence on the smectite charge and the type of the interlayer cation (dashed lines in Figure 11a). The number of H bonds donated to basal oxygen atoms was ~ 2.0 per H_2O molecule for the bidentate orientation and slightly <1.0 for the monodentate orientation for all types of simulated smectite systems (thick solid lines in Figure 11a). The number of H bonds per H_2O donated to other H_2O was independent of charge and interlayer cation (thin solid line in Figure 11a).

The average number of weak H bonds calculated according to the modified geometric criterion showed no substantial dependence on the type of smectite (Figure 11). The weakest H bonds ($0.8-1.0$ of donated H bonds per H_2O ; thick solid line in Figure 11b) was clearly attributed to the bidentate orientation, but some contribution from the monodentate population, amounting to ~ 0.3 donated H bonds per H_2O was also observed. For comparison, the average number of weak H bonds in bulk liquid water, calculated using the same criteria, was ~ 0.17 per molecule. Therefore, only the fraction of weak H bonds that is in excess of the value of ~ 0.17 per molecule can be considered as contributing to the sharp, high-frequency vibrational band. In agreement with the calculated power spectra, these H bonds are due solely to the bidentate and monodentate populations in the vicinity of the surface and no contribution from the central part of the interlayer was found.

CONCLUSIONS

(1) Interfacial water molecules in bidentate and monodentate orientations with respect to the siloxane surface are the only species contributing to the experimentally observed, sharp, high-frequency $O-H_w$ stretching band of smectites (Kuligiewicz *et al.*, 2015a, 2015b). The number of interlayer H_2O molecules in the monodentate orientation greatly exceeds that in the bidentate orientation and is, thus, the predominant contributor to the high-frequency vibrational band.

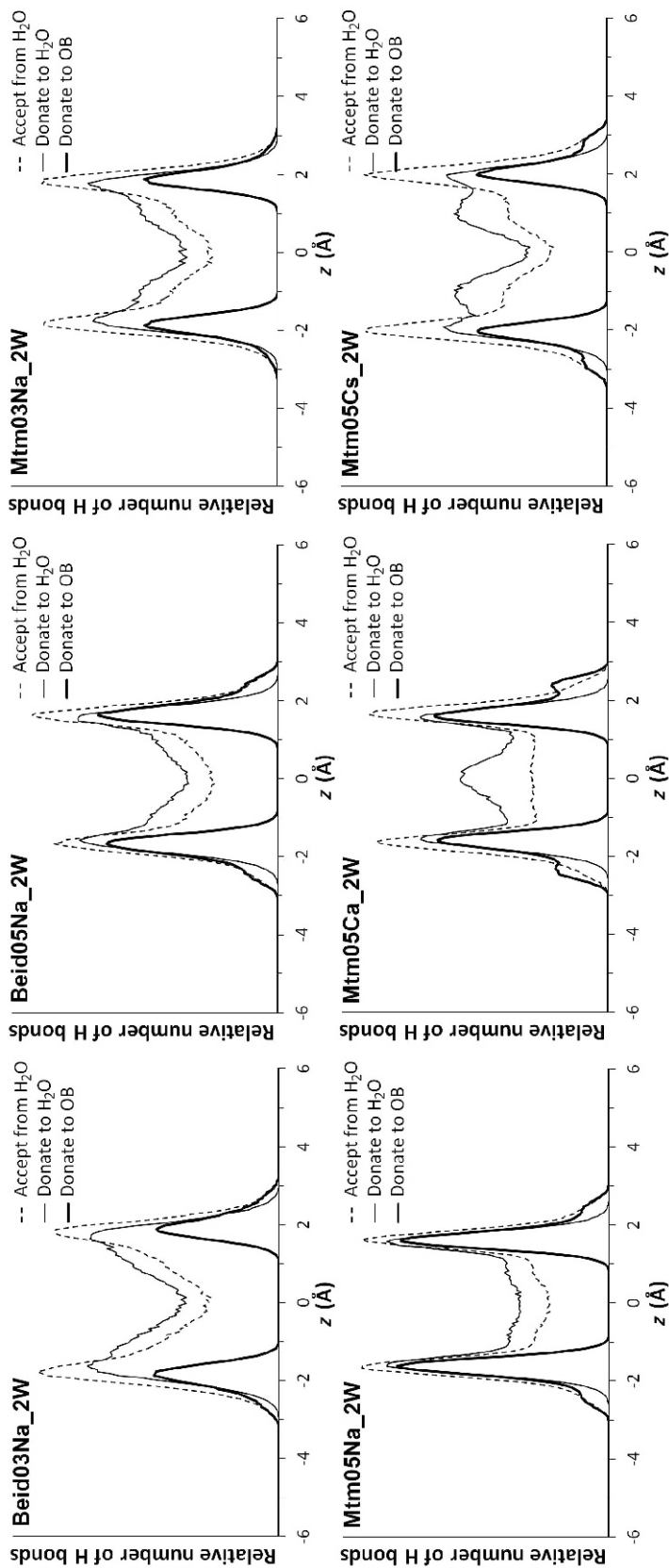


Figure 10. Distributions of O_w atoms with H bonds accepted and donated by the interlayer H_2O and O_b in the 2W smectite structures studied.

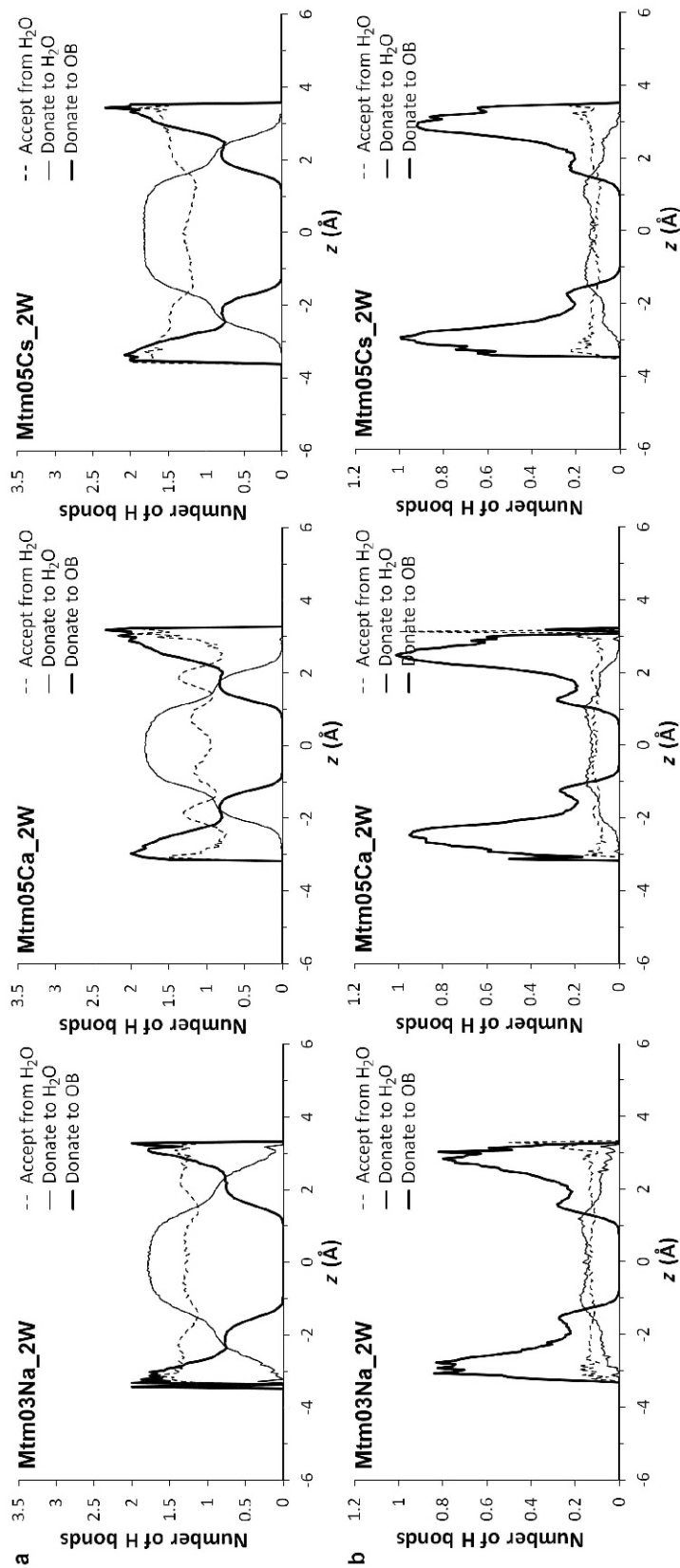


Figure 11. Distributions of O_w atoms with H bonds of various types (normalized per one H_2O) for the 2W smectite structures studied. (a) All H bonds with $O-H_w \cdots O$ distances of $<2.45 \text{ \AA}$; (b) weak (long) H bonds with $O-H_w \cdots O$ distances in the range $2.2-2.7 \text{ \AA}$. In both cases the $H_w-O \cdots O$ angle is $<30^\circ$.

(2) In the bidentate orientation, each H₂O molecule donates two hydrogen bonds to the surface: one relatively strong, and another much weaker, while in the monodentate orientation it donates only one relatively weak H bond to the surface.

(3) Increasing the total layer charge leads to an increasing number of bidentate molecules, but also to decreasing O–H_w⋯O_b distances for both monodentate and bidentate populations. Both factors are responsible for the red-shift of the sharp, high-frequency band in smectites upon increase of the layer charge.

(4) The experimentally observed low sensitivity of the position of the high-frequency vibrational band on the type of the (Na⁺ or Ca²⁺) high hydration enthalpy interlayer cation remains unexplained. The differentiation of Cs⁺ from Na⁺ or Ca²⁺ may be due to its tendency to displace surface H₂O and form inner-sphere complexes with the siloxane surface as suggested by Kuligiewicz *et al.* (2015a), but further simulation work is needed to account for the experimental data on Cs⁺ smectites.

(5) The presence of the sharp, high-frequency vibrational band in experimental and simulated spectra can be considered as strong evidence of intrinsic hydrophobicity of the smectite siloxane surface within the studied range of layer charge (0.3–0.5 p.h.u.c.), independent of the specific charge localization in the clay structure.

ACKNOWLEDGMENTS

The present work was supported by the project ATLAB (FP7-REGPOT-2011-1 No. 285989) funded by the European Union. MS also acknowledges NCN (grant 2012/05/B/ST10/01948), which provided IGS PAS with a high-performance computing server and also PLGRID infrastructure. AGK acknowledges the support of the industrial chair “Storage and Disposal of Radioactive Waste” at the Ecole des Mines de Nantes, funded by ANDRA, Areva, and EDF. VG and GDC acknowledge partial support from project KRHPIS 447963-Polynano (GSRT, TPCI-NHRF).

REFERENCES

Allen, M.P. and Tildesley, D.J. (1987) *Computer Simulation of Liquids*. Oxford University Press, New York, 385 pp.

Arab, M., Bougeard, D., and Smirnov, K.S. (2003) Structure and dynamics of the interlayer water in an uncharged 2:1 clay. *Physical Chemistry Chemical Physics*, **5**, 4699–4707.

Boek, E.S. and Sprik, M. (2003) Ab initio molecular dynamics study of the hydration of a sodium smectite clay. *Journal of Physical Chemistry B*, **107**, 3251–3256.

Boek, E.S., Coveney, P.V., and Skipper, N.T. (1995) Monte Carlo molecular modeling studies of hydrated Li-, Na-, and K-smectites: Understanding the role of potassium as a clay swelling inhibitor. *Journal of the American Chemical Society*, **117**, 12608–12617.

Bridgeman, C.H. and Skipper, N.T. (1997) A Monte Carlo study of water at an uncharged clay surface. *Journal of Physics-Condensed Matter*, **9**, 4081–4087.

Cariati, F., Erre, L., Micera, G., Piu, P., and Gessa, C. (1981) Water molecules and hydroxyl groups in montmorillonites as studied by near infrared spectroscopy. *Clays and Clay*

Minerals, **29**, 157–159.

Cariati, F., Erre, L., Micera, G., Piu, P., and Gessa, C. (1983) Polarization of water molecules in phyllosilicates in relation to exchange cations as studied by near infrared spectroscopy. *Clays and Clay Minerals*, **31**, 155–157.

Cases, J.M., Berend, L., Francois, M., Uriot, J.P., Michot, L.J., and Thomas, F. (1997) Mechanism of adsorption and desorption of water vapor by homoionic montmorillonite. 3. The Mg²⁺, Ca²⁺, Sr²⁺ and Ba²⁺ exchanged forms. *Clays and Clay Minerals*, **45**, 8–22.

Chang, F.R.C., Skipper, N.T., and Sposito, G. (1995) Computer simulation of interlayer molecular structure in sodium montmorillonite hydrates. *Langmuir*, **11**, 2734–2741.

Churakov, S.V. (2006) Ab initio study of sorption on pyrophyllite: Structure and acidity of the edge sites. *Journal of Physical Chemistry B*, **110**, 4135–4146.

Cygan, R.T., Liang, J.J., and Kalinichev, A.G. (2004) Molecular models of hydroxide, oxyhydroxide, and clay phases and the development of a general force field. *Journal of Physical Chemistry B*, **108**, 1255–1266.

Dazas, B., Ferrage, E., Delville, A., and Lanson, B. (2014) Interlayer structure model of tri-hydrated low-charge smectite by X-ray diffraction and Monte Carlo modeling in the Grand Canonical ensemble. *American Mineralogist*, **99**, 1724–1735.

Dazas, B., Lanson, B., Delville, A., Robert, J.L., Komarneni, S., Michot, L.J., and Ferrage, E. (2015) Influence of tetrahedral layer charge on the organization of interlayer water and ions in synthetic Na-saturated smectites. *Journal of Physical Chemistry C*, **119**, 4158–4172.

Efimov, Y.Y. and Naberhukhin, Y.I. (2002) On the interrelation between frequencies of stretching and bending vibrations in liquid water. *Spectrochimica Acta A*, **58**, 519–524.

Farmer, V.C. and Russell, J.D. (1971) Interlayer complexes in layer silicates: The structure of water in lamellar ionic solutions. *Transactions of the Faraday Society*, **67**, 2737–2749.

Ferrage, E., Lanson, B., Sakharov, B.A., and Drits, V.A. (2005) Investigation of smectite hydration properties by modeling experimental X-ray diffraction patterns: Part I. Montmorillonite hydration properties. *American Mineralogist*, **90**, 1358–1374.

Ferrage, E., Lanson, B., Sakharov, B.A., Geoffroy, N., Jacquot, E., and Drits, V.A. (2007) Investigation of dioctahedral smectite hydration properties by modeling of X-ray diffraction profiles: Influence of layer charge and charge location. *American Mineralogist*, **92**, 1731–1743.

Ferrage, E., Sakharov, B.A., Michot, L.J., Delville, A., Bauer, A., Lanson, B., Grangeon, S., Frapper, G., Jiménez-Ruiz, M., and Cuello, G.J. (2011) Hydration properties and interlayer organization of water and ions in synthetic Na-smectite with tetrahedral layer charge. Part 2. Toward a precise coupling between molecular simulations and diffraction data. *Journal of Physical Chemistry C*, **115**, 1867–1881.

Greathouse, J.A. and Sposito, G. (1998) Monte Carlo and molecular dynamics studies of interlayer structure in Li(H₂O)₃-smectites. *Journal of Physical Chemistry B*, **102**, 2406–2414.

Greathouse, J.A., Durkin, J.S., Larentzos, J.P., and Cygan, R.T. (2009) Implementation of a Morse potential to model hydroxyl behavior in phyllosilicates. *Journal of Chemical Physics*, **130**, 134713.

Greathouse, J.A., Hart, D.B., Bowers, G.M., Kirkpatrick, R.J., and Cygan, R.T. (2015) Molecular simulation of structure and diffusion at smectite-water interfaces: Using expanded clay interlayers as model nanopores. *Journal of Physical Chemistry C*, **119**, 17126–17136.

- Guillot, B. (2002) A reappraisal of what we have learnt during three decades of computer simulations on water. *Journal of Molecular Liquids*, **101**, 219–260.
- Jaynes, W.F. and Boyd, S.A. (1991) Hydrophobicity of siloxane surfaces in smectites as revealed by aromatic hydrocarbon adsorption from water. *Clays and Clay Minerals*, **39**, 428–436.
- Kalinichev, A.G. (2001) Molecular simulations of liquid and supercritical water: Thermodynamics, structure, and hydrogen bonding. Pp. 83–129 in: *Molecular Modeling Theory: Applications in the Geosciences* (R.T. Cygan and J.D. Kubicki, editors). Reviews in Mineralogy and Geochemistry, **42**, Mineralogical Society of America, Washington, D.C.
- Kleinhesselink, D. and Wolfsberg, M. (1992) The evaluation of power spectra in molecular dynamics simulations of anharmonic solids and surfaces. *Surface Science*, **262**, 189–207.
- Kuligiewicz, A., Derkowski, A., Szczerba, M., Gionis, V., and Chryssikos, G.D. (2015a) Water–smectite interface by infrared spectroscopy. *Clays and Clay Minerals*, **63**, 15–29.
- Kuligiewicz, A., Derkowski, A., Emmerich, K., Christidis, G.E., Tsiantos, C., Gionis, V., and Chryssikos, G.D. (2015b) Measuring the layer charge of dioctahedral smectite by O–D vibrational spectroscopy. *Clays and Clay Minerals*, **63**, 443–456.
- Kumar, R., Schmidt, J.R., and Skinner, J.L. (2007) Hydrogen bonding definitions and dynamics in liquid water. *Journal of Chemical Physics*, **126**, 204107–204112.
- Lee, J.H. and Guggenheim, S. (1981) Single crystal X-ray refinement of pyrophyllite-1Tc. *American Mineralogist*, **66**, 350–357.
- Libowitzky, E. (1999) Correlation of O–H stretching frequencies and O–H...O bond lengths in minerals. *Monatshefte für Chemie*, **130**, 1047–1059.
- Loganathan, N. and Kalinichev, A.G. (2013) On the hydrogen bonding structure at the aqueous interface of ammonium-substituted mica: A molecular dynamics simulation. *Zeitschrift für Naturforschung A*, **68**, 91–100.
- Loganathan, N., Yazaydin, A.O., Bowers, G.M., Kalinichev, A.G., and Kirkpatrick, R.J. (2016a) Structure, energetics, and dynamics of Cs⁺ and H₂O in hectorite: Molecular dynamics simulations with an unconstrained substrate surface. *Journal of Physical Chemistry C*, **120**, 10298–10310.
- Loganathan, N., Yazaydin, A.O., Bowers, G.M., Kalinichev, A.G., and Kirkpatrick, R.J. (2016b) Cation and water structure, dynamics, and energetics in smectite clays: A molecular dynamics study of Ca-hectorite. *Journal of Physical Chemistry C*, **120**, 12429–12439.
- Löwenstein, W. (1954) The distribution of aluminum in the tetrahedra of silicates and aluminates. *American Mineralogist*, **39**, 92–96.
- Madejová, J., Janek, M., Komadel, P., Herbert, H.-J., and Moog, H.C. (2002) FTIR analyses of water in MX-80 bentonite compacted from high salinity salt solution systems. *Applied Clay Science*, **20**, 255–271.
- Marry, V., Rotenberg, B., and Turq, P. (2008) Structure and dynamics of water at a clay surface from molecular dynamics simulation. *Physical Chemistry Chemical Physics*, **10**, 4802–4813.
- Marry, V., Dubois, E., Malikova, N., Brey, J., and Haussler, W. (2013) Anisotropy of water dynamics in clays: Insights from molecular simulations for experimental QENS analysis. *Journal of Physical Chemistry C*, **117**, 15106–15115.
- Michot, L.J., Villieras, F., Francois, M., Yvon, J., Le Dred, R., and Cases, J.M. (1994) The structural microscopic hydrophilicity of talc. *Langmuir*, **10**, 3765–3773.
- Morrow, C.P., Yazaydin, A.O., Krishnan, M., Bowers, G.M., Kalinichev, A.G., and Kirkpatrick, R.J. (2013) Structure, energetics, and dynamics of smectite clay interlayer hydration: molecular dynamics and metadynamics investigation of Na-hectorite. *Journal of Physical Chemistry C*, **117**, 5172–5187.
- Ngouana Wakou, B.F. and Kalinichev, A.G. (2014) Structural arrangements of isomorphous substitutions in smectites: Molecular simulation of the swelling properties, interlayer structure, and dynamics of hydrated Cs–montmorillonite revisited with new clay models. *Journal of Physical Chemistry C*, **118**, 12758–12773.
- Ortega-Castro, J., Hernández-Haro, N., Dove, M.T., Hernández-Laguna, A., and Sainz-Diaz, C.I. (2010) Density functional theory and Monte Carlo study of octahedral cation ordering of Al/Fe/Mg cations in dioctahedral 2:1 phyllosilicates. *American Mineralogist*, **95**, 209–220.
- Plimpton, S. (1995) Fast parallel algorithms for short-range molecular dynamics. *Journal of Computational Physics*, **117**, 1–19.
- Praprotnik, M., Janezic, D., and Mavri, J. (2004) Temperature dependence of water vibrational spectrum: A molecular dynamics simulation study. *Journal of Physical Chemistry A*, **108**, 11056–11062.
- Prost, R. (1975) Interactions between adsorbed water molecules and the structure of clay minerals: Hydration mechanism of smectites. *Proceedings of the International Clay Conference of The Clay Minerals Society, Mexico City*, 351–359.
- Rotenberg, B., Patel, A.J., and Chandler, D. (2011) Molecular explanation for why talc surfaces can be both hydrophilic and hydrophobic. *Journal of the American Chemical Society*, **133**, 20521–20527.
- Russell, J.D. and Farmer, V.C. (1964) Infrared spectroscopic study of the dehydration of montmorillonite and saponite. *Clay Minerals Bulletin*, **5**, 443–464.
- Sato, T., Watanabe, T., and Otsuka, R. (1992) Effects of layer charge, charge location, and energy change on expansion properties of dioctahedral smectites. *Clays and Clay Minerals*, **40**, 103–113.
- Skipper, N.T., Soper, A.K., and McConnell, J.D.C. (1991) The structure of interlayer water in vermiculite. *Journal of Chemical Physics*, **94**, 5751–5760.
- Sobolev, O., Favre Buivin, F., Kemner, E., Russina, M., Beuneu, B., Cuello, G.J., and Charlet, L. (2010) Water-clay surface interaction: A neutron scattering study. *Chemical Physics*, **374**, 55–61.
- Šolc, R., Gerzabek, M.H., Lischka, H., and Tunega, D. (2011) Wettability of kaolinite (001) surfaces – molecular dynamic study. *Geoderma*, **169**, 47–54.
- Sovago, M., Kramer Campen, R.K., Bakker H.J., and Bonn, M. (2009) Hydrogen bonding strength of interfacial water determined with surface sum-frequency generation. *Chemical Physics Letters*, **470**, 7–12.
- Sposito, G. and Prost, R. (1982) Structure of water adsorbed on smectites. *Chemical Reviews*, **82**, 554–573.
- Sposito, G., Prost, R., and Gaultier, J.-P. (1983) Infrared spectroscopic study of adsorbed water on reduced-charge Na/Li-montmorillonites. *Clays and Clay Minerals*, **31**, 9–16.
- Sposito, G., Skipper, N.T., Sutton, R., Park, S.-H., Soper, A.K., and Greathouse, J.A. (1999) Surface geochemistry of clay minerals. *Proceedings of the National Academy of Science USA*, **96**, 3358–3364.
- Suquet, H., Prost, R., and Pezerat, H. (1977) Etude par la spectroscopie infrarouge de l'eau adsorbée par la saponite-calcium. *Clay Minerals*, **12**, 113–125.
- Suzuki, S. and Kawamura, K. (2004) Study of vibrational spectra of interlayer water in sodium beidellite by molecular dynamics simulations. *Journal of Physical Chemistry B*,

- 108, 13468–13474.
- Środoń, J. and McCarty, D.K. (2008) Surface area and layer charge of smectite from CEC and EGME/H₂O retention measurements. *Clays and Clay Minerals*, **56**, 155–174.
- Szczerba, M., Kłapyta, Z., and Kalinichev, A.G. (2014) Ethylene glycol intercalation in smectites. Molecular dynamics simulation studies. *Applied Clay Science*, **91**, 87–97.
- Tay, K. and Bresme, F. (2006) Hydrogen bond structure and vibrational spectrum of water at a passivated metal nanoparticle. *Journal of Materials Chemistry*, **16**, 1956–1962.
- Teich-McGoldrick, S.L., Greathouse, J.A., Jové-Colón, C.F., and Cygan, R.T. (2015) Swelling properties of montmorillonite and beidellite clay minerals from molecular simulation: Comparison of temperature, interlayer cation, and charge location effects. *Journal of Physical Chemistry C*, **119**, 20880–20891.
- Toukan, K. and Rahman, A. (1985) Molecular-dynamics study of atomic motions in water. *Physical Review B*, **31**, 2643–2648.
- Tunega, D., Gerzabek, M.H. and Lischka, H. (2004) Ab initio molecular dynamics study of a monomolecular water layer on octahedral and tetrahedral kaolinite surfaces. *Journal of Physical Chemistry B*, **108**, 5930–5936.
- Wang, J.W., Kalinichev, A.G., and Kirkpatrick, R.J. (2004) Molecular modeling of the 10-angstrom phase at subduction zone conditions. *Earth and Planetary Science Letters*, **222**, 517–527.
- Wang, J.W., Kalinichev, A.G., and Kirkpatrick, R.J. (2005a) Structure and decompression melting of a novel, high-pressure nanoconfined 2-D ice. *Journal of Physical Chemistry B*, **109**, 14308–14313.
- Wang, J., Kalinichev, A.G., Kirkpatrick, R.J., and Cygan, R.T. (2005b) Structure, energetics, and dynamics of water adsorbed on the muscovite (001) surface: a molecular dynamics simulation. *The Journal of Physical Chemistry B*, **109**, 15893–15905.
- Wang, J., Kalinichev, A.G., and Kirkpatrick, R.J. (2009) Asymmetric hydrogen bonding and orientational ordering of water at hydrophobic and hydrophilic surfaces: A comparison of water/vapor, water/talc, and water/mica interfaces. *Journal of Physical Chemistry C*, **113**, 11077–11085.
- Xu, W., Johnston, C.T., Parker, P., and Agnew, S.F. (2000) Infrared study of water sorption on Na-, Li-, Ca- and Mg-exchanged (SWy-1 and SAz-1) montmorillonite. *Clays and Clay Minerals*, **48**, 120–131.
- Zaunbrecher, L.K., Cygan, R.T., and Elliott, W.C. (2015) Molecular models of cesium and rubidium adsorption on weathered micaceous minerals. *Journal of Physical Chemistry A*, **119**, 5691–5700.

(Received 12 February 2016; revised 1 July 2016; Ms. 1090; AE: Xiandong Liu)